



Title	Microstructure and Toughness in Weld Heat-Affected Zone of Duplex Stainless Steel(Materials, Metallurgy & Weldability)
Author(s)	Enjo, Toshio; Kuroda, Toshio; Imanishi, Ryusuke
Citation	Transactions of JWRI. 1988, 17(2), p. 385-391
Version Type	VoR
URL	<a href="https://doi.org/10.18910/8373">https://doi.org/10.18910/8373</a>
rights	
Note	

*The University of Osaka Institutional Knowledge Archive : OUKA*

<https://ir.library.osaka-u.ac.jp/>

The University of Osaka

# Microstructure and Toughness in Weld Heat-Affected Zone of Duplex Stainless Steel†

Toshio ENJO\*, Toshio KURODA\*\* and Ryusuke IMANISHI\*\*\*

## Abstract

Relation between microstructure and toughness in weld heat affected zones of SUS329J1 duplex stainless steel has been investigated by means of fractography.

Base metal of SUS329J1 has duplex microstructure consisting of  $\alpha$  phase and elongated  $\gamma$  phase.

The upper shelf energy in the Charpy impact value versus temperature curve was affected by the location of V notch of Charpy impact specimen. For the specimen occurring crack propagation to the short transverse direction, the energy was highest, because of the presence of the platelet and elongated  $\gamma$  phase.

The presence of  $\gamma$  phase extremely causes the increase of the toughness for the ductile fracture. But the brittle fracture was hardly affected by the  $\gamma$  phase.

For the microstructure of weld heat affected zones, the specimen heated up to 1373 K has  $\alpha + \gamma$  duplex microstructure and was similar to that of the base metal. The Charpy impact value was also similar to that of the base metal.

For the specimen heated at 1473 K and 1573 K such as weld bond region, the toughness considerably decreased, because of the large grain size, the decrease of the volume fraction of  $\gamma$  phase and the precipitation of  $\text{Cr}_2\text{N}$  in the  $\alpha$  phase.

**KEY WORDS :** (Duplex Stainless Steel) (Microstructure) (Welds) (Toughness) (Transmission Electron Microscopy) (Fractography)

## 1. Introduction

SUS329J1 duplex stainless steel has been widely used for various chemical plants, because of the good resistance to corrosion and stress corrosion cracking<sup>1-3</sup>. This alloy has duplex microstructure consisting of the  $\alpha$  phase and elongated  $\gamma$  phase, and causes the increase of the toughness in comparison of the ferritic stainless steel<sup>4-8</sup>. However, the role of the  $\gamma$  phase in the toughness of duplex stainless steel has not been clearly yet.

As the duplex stainless steel is welded, the microstructure change occurs in the heat affected zone (HAZ) of the welds, and occurs the decrease in the toughness<sup>8</sup>.

But, the relation between the microstructure and toughness in the heat affected zone has not been clearly yet. Then in this paper, the microstructure of the weld heat affected zone has investigated by means of transmission electron microscopy in details and the role of the microstructure on the toughness was discussed by means of fractography.

## 2. Experimental Procedures

The chemical compositions of SUS329J1 stainless steel are shown in Table 1. The thickness of the plate was 15 mm. In order to investigate the toughness of the as-received base metal, which has heterogeneous microstructure consisting of  $\alpha$  phase and elongated  $\gamma$  phase, the V notch of the Charpy impact specimen was located to the longitudinal plane, transverse plane and thickness plane. The microstructure of the weld heat affected zone was made by the heat treatment. Namely, the specimens were heated at 1173 K, 1473 K and 1573 K for 1.8 ks respectively, and water-quenched. The toughness of the specimen was evaluated by the Charpy impact test.

The fracture surface after the impact test was observed in details using scanning electron microscopy. The micro-

Table 1 Chemical compositions of SUS329J1 steel (mass%).

C	Si	Mn	P	S	Cr	Ni	Mo	N
0.016	0.52	0.26	0.044	0.013	24.63	4.21	1.84	0.146

† Received on October 31, 1988

\* Professor

\*\* Research Instructor

\*\*\* Co-research Worker (Industrial Research Institute, Aichi Prefectural Government)

structure was revealed by the electropolishing in the 10% oxalic acid solution and the observation of precipitates was carried out by transmission electron microscopy and the identification of the precipitates and the volume fraction of the  $\alpha$  and  $\gamma$  phase were evaluated by X-ray diffraction technique using Cu K $\alpha$  filtered by nickel.

### 3. Results and Discussion

#### 3.1 Microstructure in the weld heat affected zone

Figure 1 shows the microstructure of each plane in the plate of the as-received base metal. The elongated and platelet  $\gamma$  phase is present in the  $\alpha$  phase matrix. The volume fraction of each plane was measured by X-ray diffraction method, the mean volume fraction of the  $\alpha$  phase and  $\gamma$  phase was 55% and 45% respectively.

Figure 2 shows optical microstructures of the specimens heated at 1173 K, 1473 K and 1573 K for 3.6 ks and

water-quenched.

For the specimen heat-treated at 1173 K, elongated and platelet  $\gamma$  phases are present in the  $\alpha$  phase matrix, and the microstructure is almost as same as that of as-received base metal shown in Fig. 1.

For the specimen heat-treated at 1473 K, the size of the  $\gamma$  phase becomes larger, and the number becomes more, in comparison of the specimen heat-treated at 1173 K. The volume fraction of the  $\gamma$  phase was 28% by means of X-ray diffraction technique. The fine precipitates are present in the  $\alpha$  phase matrix, and  $\alpha$  grain boundary is observed clearly.

For the specimen heat-treated at 1573 K, the fine precipitates in the  $\alpha$  phase matrix are much more than that of the specimen heat-treated at 1473 K. The volume fraction of the  $\gamma$  phase was 5% by means of X-ray diffraction technique. The grain growth of the  $\alpha$  phase occurs, and continuously film-like  $\gamma$  phase is present at the grain boundary of the  $\alpha$  phase. The white band near the grain boundary is precipitation free zones (PFZ).

Figure 3 indicates transmission electron micrographs, as the specimen was heat-treated at 1473 K. The grain boundary precipitates of rod type is observed as shown in Fig.3-(a), the precipitates was identified as Cr<sub>2</sub>N by selected area electron diffraction pattern. The plate like precipitates are also observed within the grain as shown in Fig.3-(b). The precipitates was hardly observed for the specimen heat-treated at 1173 K and as-received base metal.

Figure 4 indicates X-ray line profiles of the extraction residue of the specimen heat-treated at 1473 K. Fig. 4-(a) shows blank test of the filter paper, and Fig. 4-(b) is the result of the filter with the extraction residue. Many peaks

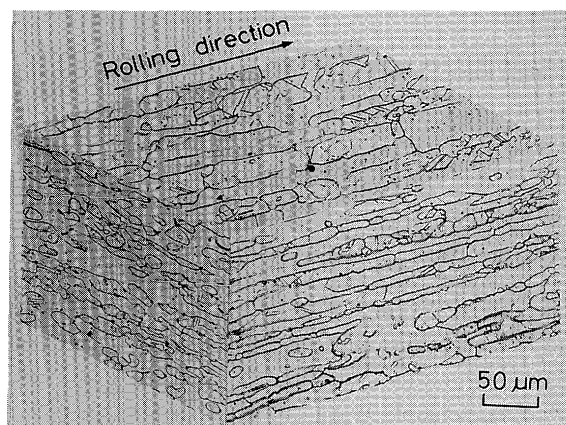


Fig. 1 Microstructure of SUS329J1 steel.

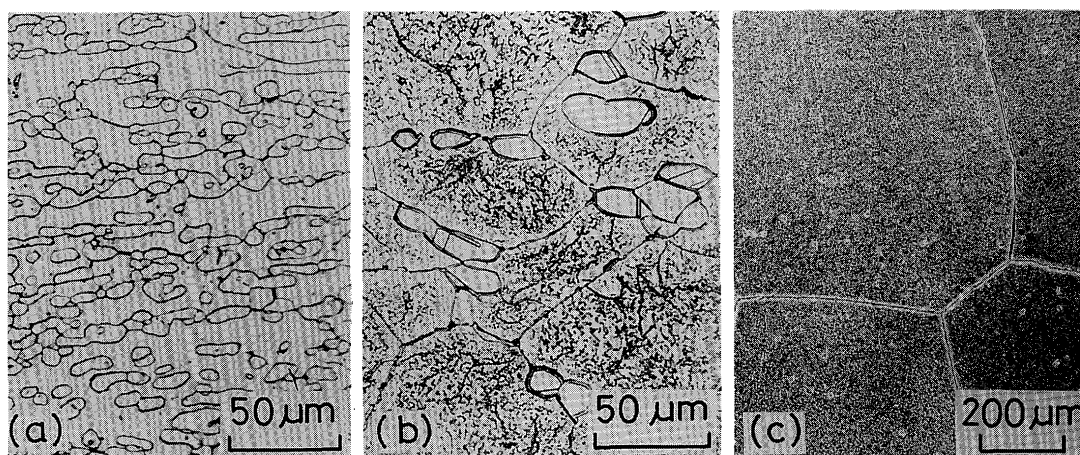


Fig. 2 Microstructure of specimens heat-treated at various temperatures.  
(a): 1173 K, (b): 1473 K, (c): 1573 K

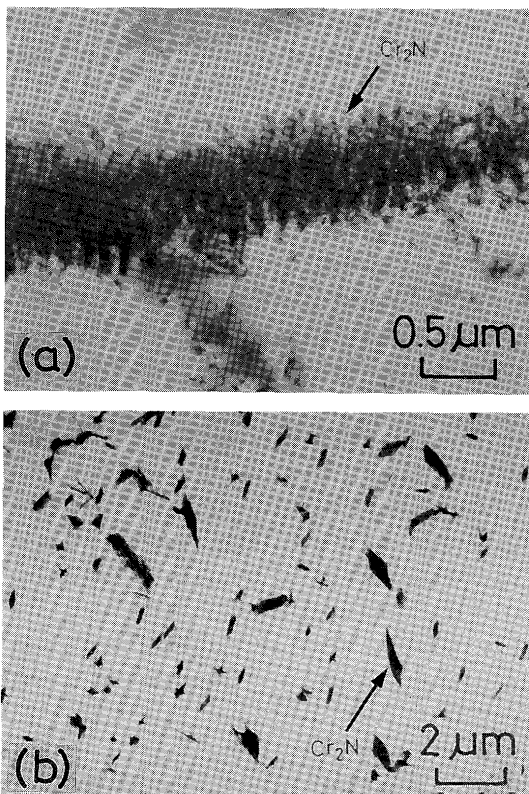


Fig. 3 Transmission electron micrographs of the specimen heat-treated at 1473 K.  
(a): Grain boundary, (b): within grain

due to the presence of  $\text{Cr}_2\text{N}$  are observed according to the ASTM card (27-127).

Generally, nitrogen is added to the duplex stainless steel. Nitrogen is solutionized in the  $\gamma$  phase for the duplex microstructure of as-received base metal<sup>1)</sup>. As the specimen is heated above 1473 K, the volume fraction of the  $\gamma$  phase decreases, and nitrogen in the  $\gamma$  phase is swept out to the  $\alpha$  phase by the  $\gamma$ - $\alpha$  transformation. But the solubility of nitrogen in the  $\alpha'$  phase is very small, so that nitrogen precipitates as  $\text{Cr}_2\text{N}$  in the  $\alpha$  phase and at the grain boundary.

Consequently, for the  $\alpha/\gamma$  duplex stainless steel heated above 1473 K, the grain growth of the  $\gamma$  phase occurs, and volume fraction of the  $\alpha$  phase is very small, and then  $\text{Cr}_2\text{N}$  precipitates in the  $\alpha$  grain and at the  $\alpha$  grain boundary.

### 3.2 Effect of shape and distribution of $\gamma$ phase on toughness

SUS329J1 steel has duplex microstructure consisting of elongated  $\gamma$  phase and  $\alpha$  phase. As the crack propagates across the  $\gamma$  phase, the crossing angle of the crack and  $\gamma$  phase is considered to affect the toughness.

Figure 5 indicates Charpy impact value versus temper-

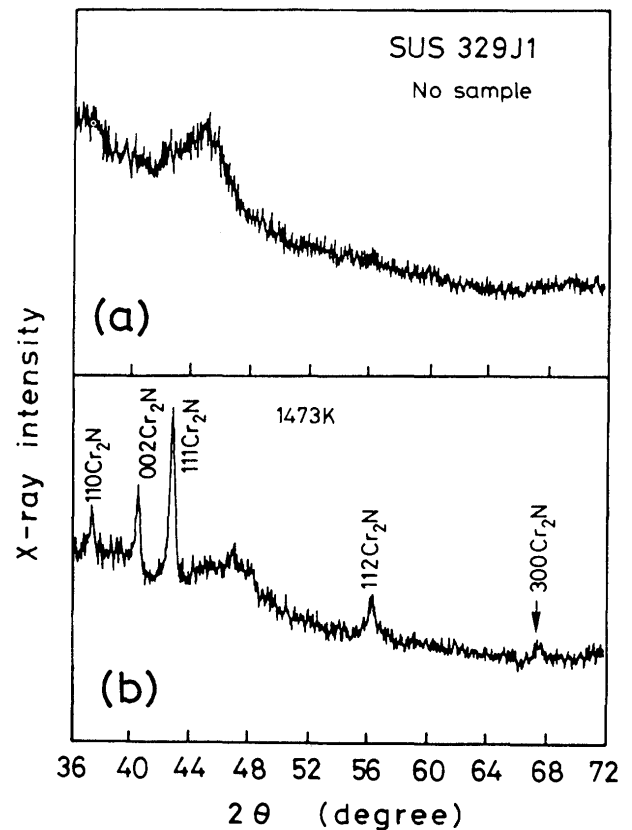


Fig. 4 X-ray diffraction pattern of the specimen heat-treated at 1473 K by extraction residue.

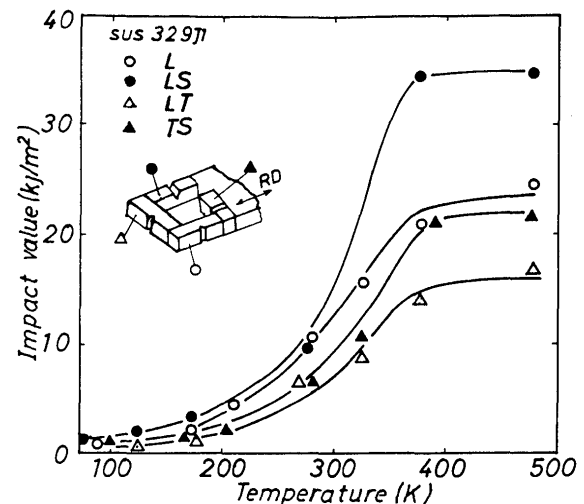


Fig. 5 Charpy impact value versus temperature curves of specimens with various notch positions.

ature curves, as the specimen with various notch location was tested.

For the upper shelf energy in the testing temperature above 373 K, the toughness of the LS direction specimen is highest, and that of the LT direction specimen is lowest.

For the LS direction specimen, the crack propagates across the wide plane of the  $\gamma$  phase. For the LT direction specimen, the crack propagates across the narrow plane of the  $\gamma$  phase.

Consequently, the shape and distribution of the  $\gamma$  phase plays an important role on the toughness of the ductile fracture.

The effect of the shape and distribution of the  $\gamma$  phase on the toughness decreases with decreasing testing temperature. It means that the decrease of the testing temperature causes the cleavage fracture of the  $\alpha$  phase matrix. The toughness at 78 K is independent of the notch portion.

**Figure 6** shows the relation between microstructure and fracture morphology for the LS direction specimen and the LT direction specimen. The V notch is located at the upper area of the photographs and the main crack propagates from the upper side to the bottom side of the photographs.

For the LS direction specimen, the morphology of the ductile fracture shown in Fig. 6-(b) is corresponded to the

microstructure shown in Fig. 6-(a). Consequently, large dimple is considered to occur in the  $\gamma$  phase. The ductile fracture in the  $\alpha$  phase shows small dimple, and the crack in the  $\alpha$  phase shows zig-zag fracture.

For the LT direction specimen, the morphology of the ductile fracture shown in Fig. 6-(e) is corresponded to the microstructure shown in Fig. 6-(d). Consequently, the large dimple also occurs in the  $\gamma$  phase.

Consequently, the shape and distribution of the  $\gamma$  phase affect the fracture morphology of the ductile fracture. It means that the large dimple due to the fracture of the  $\gamma$  phase occurred, prior to the fracture of the  $\alpha$  phase showing small dimple. As the crack propagates across the  $\gamma$  phase, the crack proceeds around the  $\gamma$  phase, because of the keying effects<sup>9</sup>.

The region of the cleavage fracture increases with decreasing testing temperature. The fracture region of the  $\gamma$  phase is smaller than the distribution of the  $\gamma$  phase as shown in Fig. 6-(c) and Fig. 6-(f).

In the cleavage fracture region, the fracture unit facet becomes smaller, because of the decrease of the effective

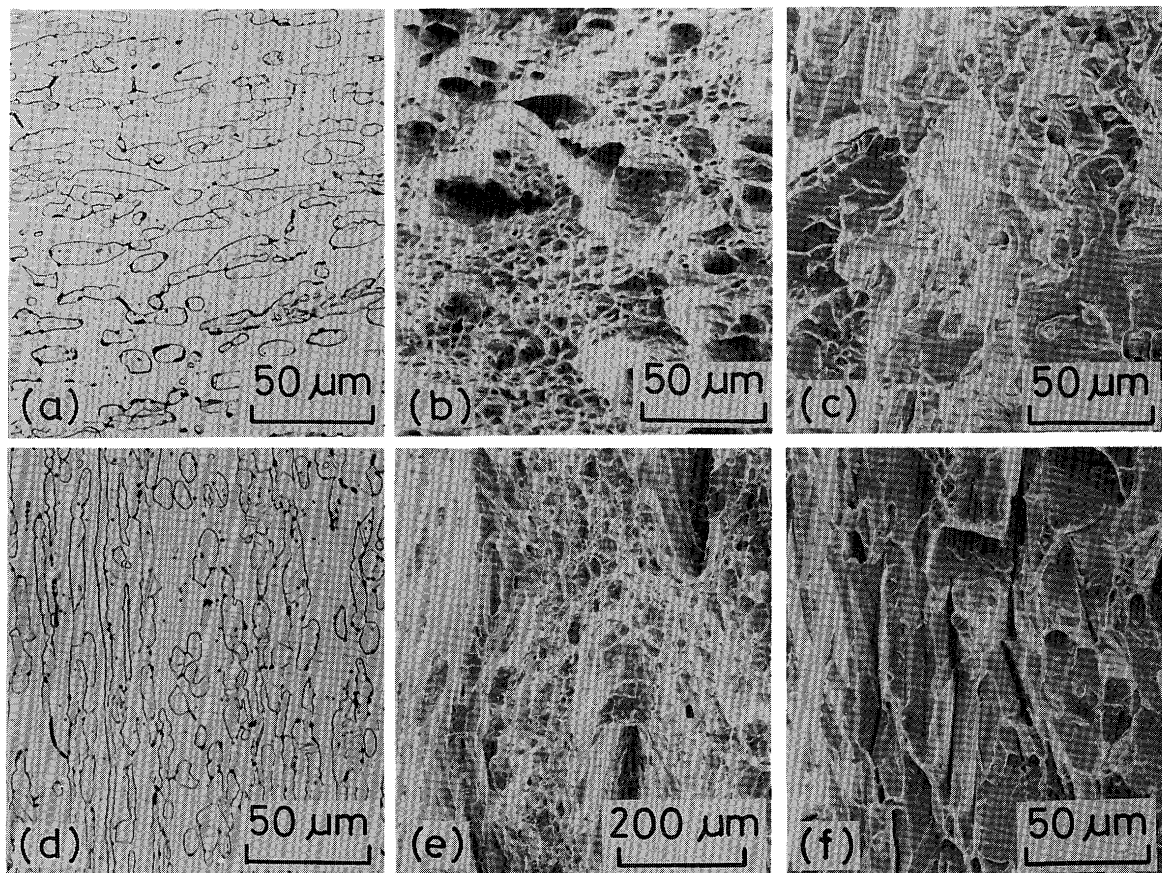


**Fig. 6** Relation between microstructure (a), (d) and fracture morphology (b), (c), (e), (f).  
(b), (e): Testing at 373 K. (c), (f): Testing at 77 K.

grain size. For the cleavage fracture, the crack propagates on the cleavage plane in crystallography. The effect of the  $\gamma$  phase is small.

The fracture of the  $\gamma$  phase occurs by the tear and shear type in order to connect the cleavage fracture of the  $\alpha$  phase, or the secondary crack occurs at the  $\alpha/\gamma$  interface.

Consequently, the effect of the  $\gamma$  phase for the cleavage fracture is smaller than that of the ductile fracture.

**Figure 7** indicates the fracture morphology at 273 K and 77 K for the L direction specimen. For the specimen tested at 273 K, the shear fracture of the  $\gamma$  phase or the separation at the  $\alpha/\gamma$  interface occurs.

For the specimen tested at 77 K, the shear fracture of the  $\gamma$  phase or the separation of the  $\alpha/\gamma$  interface occurs as the secondary crack. Consequently, the keying effect of

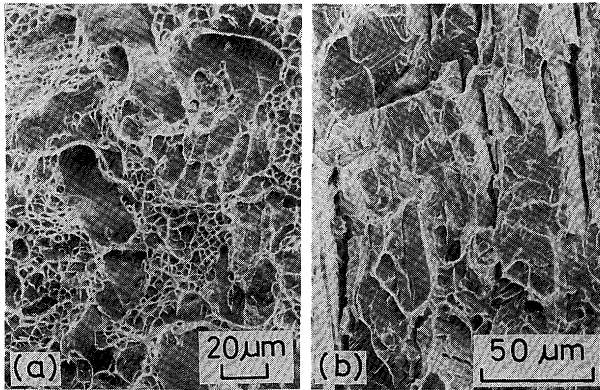


**Fig. 7** Fracture morphology of specimens.  
(a): Tested at 273 K.  
(b): Tested at 77 K.

the  $\gamma$  phase during the cleavage fracture of the  $\alpha$  phase is considered to be small.

Generally, for the ductile fracture of the duplex stainless steel, the increase of the toughness is due to the presence of the ductile  $\gamma$  phase. Namely, it is considered that the fracture of the  $\gamma$  phase occurs after the fracture of the  $\alpha$  phase. But, the fracture morphology is Fig. 6-(b), (e) and Fig. 7-(a) shows that the fracture of the  $\alpha$  phase occurs after the fracture of the  $\gamma$  phase. As the testing temperature becomes lower, the separation of  $\alpha/\gamma$  interface occurs, and the keying effect of the  $\gamma$  phase hardly occurs.

Generally, for the duplex microstructure consisting of  $\alpha$  phase and  $\gamma$  phase, the microscopic residual stress occurs due to the co-presence of the duplex microstructure. This phenomena is called as “phase stress”. Consequently, as the duplex steel is rapidly cooled from the high temperature such as solution temperature, compressive residual stress occurs in the  $\alpha$  phase with small ther-

mal expansion coefficient, and tension residual stress occurs in the  $\gamma$  phase with large thermal expansion coefficient. Consequently, it is considered that the fracture occurs at  $\alpha/\gamma$  interface. As the crack in the  $\alpha$  phase propagate across the  $\gamma$  phase, the crack propagate as the secondary crack at  $\alpha/\gamma$  interface and the crack cannot propagate through the  $\gamma$  phase. The secondary crack at  $\alpha/\gamma$  interface is crossing to the main crack in the  $\alpha$  phase. As the results, the increase of the toughness takes place as shown in Fig. 5.

Generally,  $\gamma$  phase occurs martensite transformation by the plastic deformation. In this investigation, the transformation of the  $\gamma$  phase to  $\alpha'$  phase at 373 K is small, and the  $\gamma$  phase remains after plastic deformation. The separation at  $\alpha/\gamma$  interface occurs as shown in Fig. 6-(b), (e).

The surrounding region of the  $\gamma$  phase is very flat at 273 K as shown in Fig. 7-(a). This is considered that the martensite transformation occurs and is due to the lowering the binding force of  $\alpha/\gamma$  interface.

### 3.3 Microstructure and toughness in weld heat affected zone

**Figure 8** shows Charpy impact value versus temperature curves, as the specimens were heated at various temperature and then water-quenched.

For the specimen heat-treated at 1473 K, the volume fraction of the  $\gamma$  phase is lower and the energy curve is shifted toward the high temperature side in comparison to that at 1173 K.

For the specimen heat-treated at 1573 K, the upper shelf energy is very small, the impact value is lower than that of the specimen heat-treated below 1473 K, over a wide range of the testing temperature.

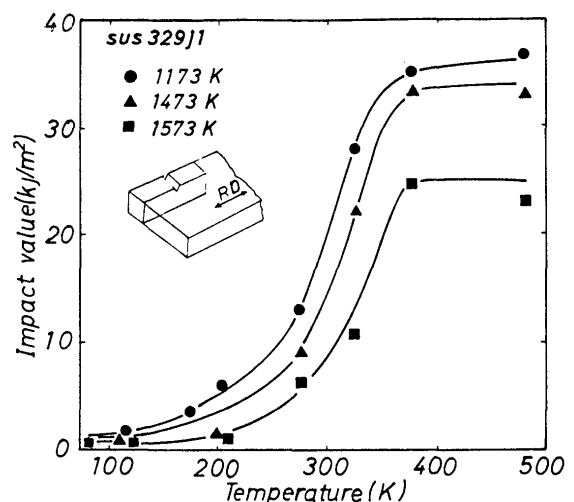


**Fig. 8** Charpy impact value versus temperature curves of heat-treated specimen.



**Figure 9** indicates the fracture morphology of the specimen impact-tested at 373 K showing upper shelf energy. For the specimen heat-treated at 1173 K, the dimple fracture occurs in the region of the  $\gamma$  phase, it is corresponded to that of as-received base metal as shown in Fig. 6-(b).

For the specimen heat-treated at 1473 K, the fracture morphology indicates the separation and secondary crack at  $\alpha / \gamma$  interface and the dimple fracture is hardly observed in the  $\gamma$  phase of the large size.

For the specimen heat-treated at 1573 K, fine precipitates of  $\text{Cr}_2\text{N}$  are present in the  $\alpha$  phase. Consequently, the fracture morphology shows small dimple as shown in Fig. 9-(c). Consequently,  $\text{Cr}_2\text{N}$  in the  $\alpha$  phase precipitates fine, and the volume fraction of the  $\gamma$  phase decreases

and the energy is lowering.

**Figure 10** shows the fracture morphology tested at 77 K, as the specimen is heated at 1173 K, 1473 K and 1573 K, and then water-quenched. The Charpy impact value at 77 K is almost same independent of the heat treatment temperature.

For the specimen heat-treated at 1173 K, the dimple and tear ridge of  $\gamma$  phase are observed on the cleavage fracture of the  $\alpha$  phase.

The crack direction of cleavage fracture is changed by the dimple fracture of the  $\gamma$  phase. But, the cleavage fracture occurs on the (100) plane in crystallography, and then the presence of the  $\gamma$  phase hardly affect the toughness.

For the specimen heat-treated at 1473 K, the region of

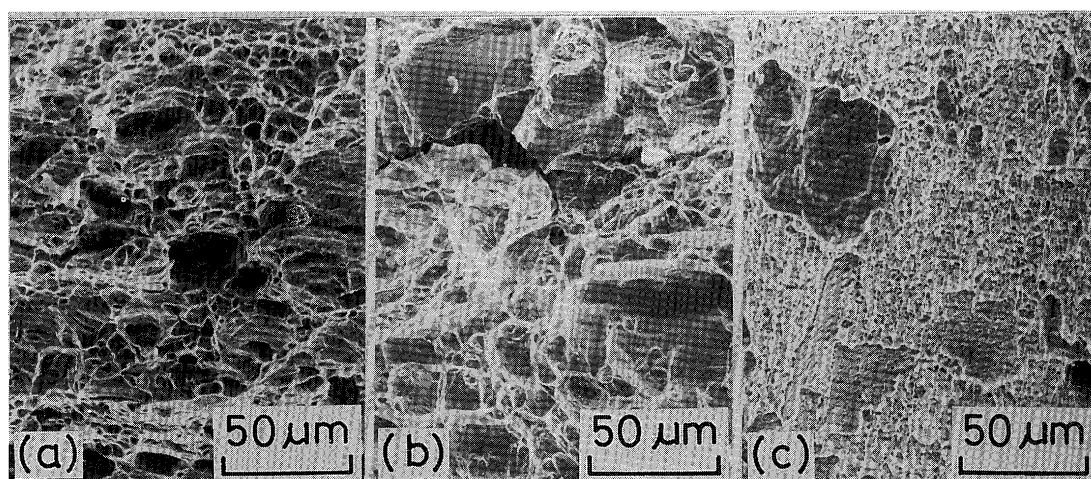


**Fig. 9** Fracture morphology of specimens tested at 373 K.  
(a): 1173 K, (b): 1473 K, (c): 1573 K

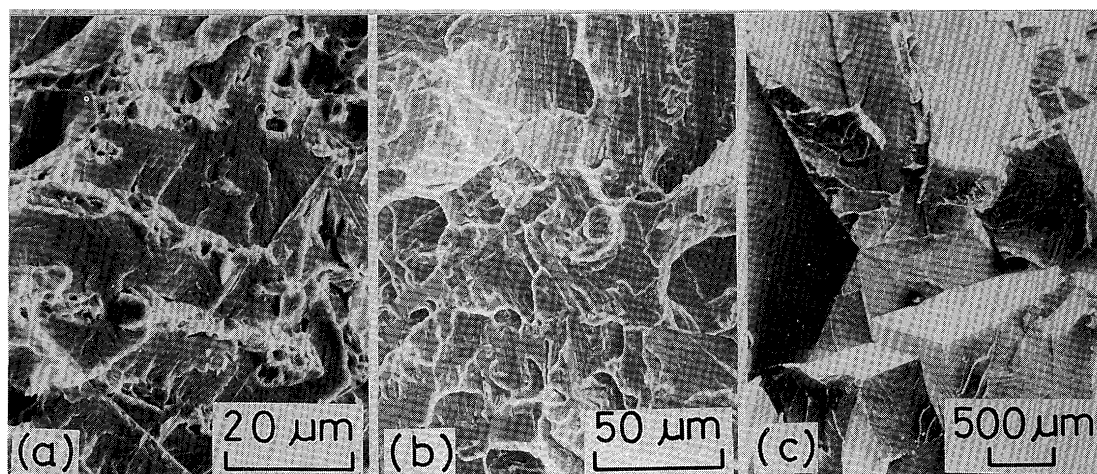


**Fig. 10** Fracture morphology of specimens tested at 77 K.  
(a): 1173 K, (b): 1473 K, (c): 1573 K

the  $\gamma$  phase is dent. It means that separation of  $\alpha/\gamma$  interface occurs.

For the specimen heat-treated at 1573 K, the grain size of the  $\alpha$  phase becomes larger. But  $\gamma$  phase precipitates at the  $\alpha$  grain boundary as shown in Fig. 2-(c). Consequently, the intergranular fracture hardly occurs. And the morphology shows cleavage fracture. The surface of the cleavage fracture is not flat. This is considered to be related to the precipitation of  $\text{Cr}_2\text{N}$  in the  $\alpha$  phase. This cleavage fracture was also observed at room temperature partially.

#### 4. Conclusion

Relation between microstructure and toughness in weld heat affected zones of SUS329J1 duplex stainless steel has been investigated by means of fractography. The results obtained in the present study are summarized as follows.

- (1) Base metal of SUS329J1 steel has duplex microstructure consisting of  $\alpha$  phase and elongated  $\gamma$  phase. The upper shelf energy in the Charpy impact value versus temperature curve was affected by the location of V notch of Charpy impact specimen. For the specimen occurring crack propagation to the short transverse direction, the energy was highest, because of the presence of the platelet and elongated  $\gamma$  phase.
- (2) The presence of  $\gamma$  phase extremely causes the increase of the toughness for the ductile fracture. But the brittle fracture was hardly affected by the  $\gamma$  phase.

- (3) For the microstructure of weld heat affected zones, the specimen heated up to 1373 K has  $\alpha + \gamma$  duplex microstructure and was similar to that of the base metal. The Charpy impact value was also similar to that of the base metal.
- (4) For the specimen heated at 1473 K and 1573 K such as weld bond region, the toughness considerably decreased, because of the large grain size, the decrease of the volume fraction of  $\gamma$  phase and the precipitation of  $\text{Cr}_2\text{N}$  in the  $\alpha$  phase.

#### References

- 1) K. Harada: Bousyoku Gijutu, 26, (1977), 721 (In Japanese)
- 2) H. Nagano and M. Kowaka: J. Iron and Steel Inst. Japan, 66, (1980), 1150 (In Japanese)
- 3) M. Kowaka, H. Nagano, T. Kudoh and K. Yamanaka: Bousyoku Gijutsu, 30, (1981), 218 (In Japanese)
- 4) A. Hoshino, K. Nakano and M. Kaneo: J. Iron and Steel Inst. Japan, 65, (1979), 70 (In Japanese)
- 5) A. Hoshino: J. Iron and Steel Inst. Japan, 72, (1986), 2279 (In Japanese)
- 6) S. Floreen, H. W. Hayden: Trans. ASM, 61, (1968), 489
- 7) I. Tamura, Y. Tomoda, Y. Yamada, S. Kanetani, M. Ozawa and A. Akao: J. Iron and Steel Inst. Japan, 59, (1973), 454 (In Japanese)
- 8) H. Izumi, H. Sunada and G. Shinoda: J. Japan Inst. Metal., 35, (1971), 454 (In Japanese)
- 9) J. W. Flowers, F. H. Beck and M. G. Fontana: Corrosion, 19, (1963), 186
- 10) Nippon zairyougakkai: X-ray ousyoku sokuteihou, (1971), 206 (In Japanese)
- 11) K. Kamachi, M. Kawano and T. Ishida: J. Iron and Steel Inst. Japan, 66, (1980), 445s (In Japanese)